Proceedings of ASME Turbo Expo 2010: Power for Land, Sea and Air
GT2010
June 14-18, 2010, Glasgow, UK

GT2010-23586

FAULT DIAGNOSIS OF GAS TURBINE ENGINES BY USING DYNAMIC NEURAL NETWORKS*

Rasul Mohammadi
Esmaeil Naderi
Khashayar Khorasani †
Shahin Hashtrudi-Zad
Department of Electrical and Computer Engineering
Concordia University
Montreal, Quebec, H3G 1M8 Canada
Email: {a_mohamm, e_naderi, kash, shz}@ece.concordia.ca

ABSTRACT

This paper presents a novel methodology for fault detection in gas turbine engines based on the concept of dynamic neural networks. The neural network structure belongs to the class of locally recurrent globally feed-forward networks. The architecture of the network is similar to the feed-forward multi-layer perceptron with the difference that the processing units include dynamic characteristics. The dynamics present in these networks make them a powerful tool useful for identification of nonlinear systems. The dynamic neural network architecture that is described in this paper is used for fault detection in a dual-spool turbo fan engine. A number of simulation studies are conducted to demonstrate and verify the advantages of our proposed neural network diagnosis methodology.

NOMENCLATURE

Variables and Constants

E	Rotor energy, J
η	Efficiency
β	Bypass ratio
W_T	Power generated by turbine, W
W_C	Power consumed by compressor, W
J	Rotor moment of inertia, $kg.m^2$
N	Rotational Speed, RPM
N_1	Rotational Speed of spool connecting high pressure compressor to high pressure turbine, RPM
N_2	Rotational Speed of spool connecting low pressure compressor to low pressure turbine, RPM
P	Pressure, Pascal
R	Gas Constant, $\frac{J}{kg.K}$
T	Temperature, K
V	Volume, m^3
$\dot{m}$	Mass flow, $\frac{kg}{s}$
π	Pressure ratio
γ	Heat capacity ratio
c_p	Specific heat at constant pressure, $\frac{J}{kg.K}$
c_v	Specific heat at constant volume, $\frac{J}{kg.K}$
H_u	Fuel specific heat, $\frac{J}{kg}$
u	Speed, $\frac{m}{s}$
A	Area, m^2
M	Mach
T_0	Temperature at sea level at Standard Day
P_0	Pressure at sea level at Standard Day

Subscripts

mech	Mechanical

*This research is supported in part by a grant from the Natural Sciences and Engineering Research Council of Canada (NSERC) under the industrial Collaborative Research and Development (CRD) partnership program.

†Address all correspondence to this author.

C	Compressor
T	Turbine
o	Stage output
i	Stage input
CC	Combustion chamber
f	Fuel
d	Intake
amb	Ambient
LT	Low pressure turbine
HT	High pressure turbine
HC	High pressure compressor
LC	Low pressure compressor
n	Nozzle
M	Mixer
n_i	Nozzle input
n_o	Nozzle output
$crit$	Critical

1 INTRODUCTION

Stringent reliability and maintainability requirements for jet engines demand development of state-of-the-art methods for fault diagnosis. There is a large body of research on health monitoring and fault diagnosis of aircraft engines (see e.g., surveys [1–4] and the references therein). Fault diagnosis in gas turbine engines has been investigated using model-free data-driven methods as well as model-based approaches. Most of the model-based approaches for fault diagnosis in aircraft engines use the continuous dynamic models and rely on analytical redundancy (see e.g. [4–7]). In [8], a model-based approach is developed for diagnosis in jet engines using hybrid automata models.

Model-based approaches are mostly based on the idea of analytical redundancy and demand an analytical mathematical model of the system. However, in practice it is usually quite challenging and difficult to meet all the requirements of model-based techniques due to the inevitable unmodeled dynamics, uncertainties, model mismatch, noise, disturbances and inherent nonlinearities. In contrast, intelligence-based diagnosis approaches such as those based on neural networks mostly rely on real-time or historical data from the engine measurements, and do not require a detailed mathematical model of the engine.

In this paper, we develop a novel neural network diagnosis methodology for the purpose of fault diagnosis in jet engines. The developed neural network is designed based on the concept of dynamic neurons. This neural network belongs to the class of locally recurrent globally feed-forward neural networks. The architecture of the network is similar to the feed-forward multilayer perceptron with the difference that the processing units include dynamic characteristics. Each dynamic neuron in our developed network consists of an adder module, a linear Finite Impulse Response (FIR) filter, and a nonlinear activation module. A powerful mapping and representational approximating tool may be obtained when dynamic neurons are connected into a multilayer structure. Since each neuron by itself possesses dynamic characteristics, no global feedback to the network structure is needed in our proposed solution. Therefore, a simpler architecture is obtained when compared to the conventional recurrent dynamic neural networks which use a global feedback in their structure. Consequently, implementing a stabilizing learning algorithm is relatively easier. Since the developed neural network has dynamic characteristics, it can be utilized for modeling and identification of general and highly complex nonlinear systems such as jet engines. We employ our dynamic neural network architecture for fault detection in a dual-spool turbo fan engine. A number of simulation studies are conducted to demonstrate and verify the advantages of our proposed neural network diagnosis methodology.

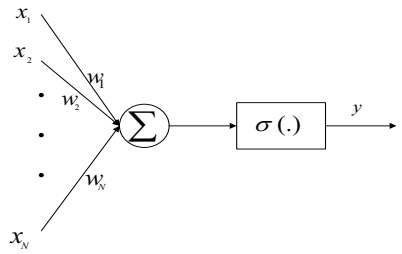

FIGURE 1. STRUCTURE OF A STATIC NEURON. [9, 10].

The remainder of the paper is organized as follows. In Section 2, we present the neural network structure used in this paper. In Section 3, the mathematical modeling of a dual-spool turbofan jet engine is investigated. The utilization of the dynamic neural network structure for fault detection in the gas turbine engine is studied in Section 4. Simulation results are presented in Section 5. We conclude the paper by presenting our conclusions in Section 6.

2 DYNAMIC NEURAL NETWORKS

In this section, we describe dynamic neural networks used in our work for fault detection of gas turbine engines. The details of the dynamic neural network for identifying different types of nonlinear systems can be found in [9, 10]. The dynamic neural network used in this paper consists of dynamic neurons. First we describe the structure of a dynamic neuron.

2.1 Dynamic Neuron with Embedded Adaptive Filter

Figure 1 shows the structure of a static neuron. In this structure, the output of the neuron is calculated by passing the weighted input $\sum_{i=1}^{N} w_i x_i$ through an activation function $\sigma(\cdot)$. In contrast to static neurons, dynamic neurons have a Finite Impulse

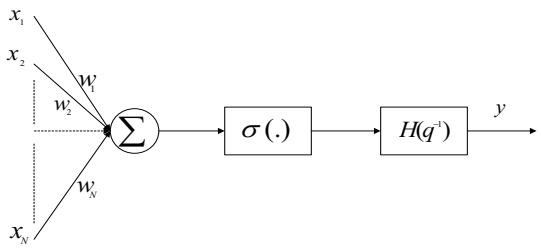

FIGURE 2. STRUCTURE OF A DYNAMIC NEURON. [9, 10].

Response (FIR) filter

$$H(q^{-1}) = \frac{1}{1 - a_1 q^{-1} - a_2 q^{-2} - \cdots a_D q^{-D}}$$

after their activation function, where D is the order of the FIR filter. The FIR filter creates a dynamic mapping between the input and the output of the neuron. Figure 2 shows the structure of a dynamic neuron. The input-output relation of the dynamic neuron is governed by

$$y(t) = \sigma(\sum_{i=1}^{N} w_i x_i) + a_1 y(t-1) + a_2 y(t-2) + \cdots a_D y(t-D),$$

where a_i's are the coefficients of the filter $H(q^{-1})$. In this work, these coefficients are also adjustable and will be updated in the training phase. The dynamic neural network in our work is constructed by using the dynamic neurons described above in a multilayer feedforward neural network. In the following, a simple neuro-dynamic structure is introduced to describe the capability of the network in identifying non-liear maps. In Section 2.4, we will present a modified structure for identifying a more general class of nonlinear systems.

2.2 The Structure of the Dynamic Neural Network

Figure 3 shows the structure of a simple dynamic neural network. This structure is similar to a multilayer perceptron, with the difference that instead of conventional static neurons, dynamic neurons have been used. The network consists of L layers with N^l neurons in layer l for $1 \leq l \leq L$. For simplicity of the discussion and without the loss of generality, only a Single-Input Single-Output (SISO) dynamic system is considered. Hence, the network has only one input and one output neurons. Any bounded, monotonically increasing and differentiable nonlinear function may be used as an activation function for the neurons. In this paper, we use a tangent hyperbolic function as the activation function. The following notation is used throughout the paper. The output of the j^{th} neuron in the l^{th} layer at time t is

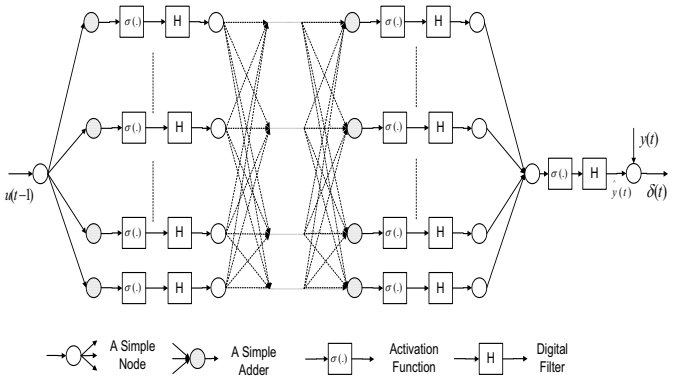

FIGURE 3. STRUCTURE OF A MULTILAYER DYNAMIC NEURAL NETWORK. [9, 10].

denoted by $o_j^l(t)$. The weight connecting the j^{th} neuron in the l^{th} layer to the i^{th} neuron in the $(l-1)^{th}$ layer is denoted by w_{ji}^l and the d^{th} filter coefficient for the j^{th} neuron in the l^{th} layer is denoted by a_{jd}^l. Here, $j \in [1 \;\; N^l]$, $i \in [1 \;\; N^{l-1}]$, $d \in [1 \;\; D]$ and $l \in [1 \;\; L]$.

It can be shown that if the order of the filter (D) and the number of layers (L) are appropriately selected, the above-mentioned dynamic neural network can be used for identification of a class of nonlinear system represented by [9, 10]

$$y(t) = \sum_{i=1}^{N_s} \alpha_i y(t-i) + g[u(t-1), u(t-2), \cdots, u(t-M_s)], \quad (1)$$

where $M_s \leq N_s$. The following inequality must hold as well $D \geq N_s$. According to the approximation theorem of [11], for approximation of any nonlinear function, the network must have at least two layers. Therefore, we must also have $L \geq 2$.

2.3 Adaptation Laws

The adaptation laws for $w's$ and $a's$ [9, 10] are derived based on the steepest descent gradient method and conventional back-propagation learning law [12]. The network parameters, namely, the neuron weights and the filter coefficients are updated so that the norm of the identification error defined as

$$E(t) = \frac{1}{2} \sum_{k=1}^{K} (y_k(t) - o_k^L(t))^2 \quad (2)$$

is minimized, where $y_k(t)$ is the k^{th} output of the network at time t.

2.3.1 Output Layer Adaptation Laws The following update laws are derived for the weights and filter parameters in the output layer [9, 10].

$$\begin{cases} \Delta w_{kj}^L = \eta\, \delta_k^L(t) \frac{\partial o_k^L(t)}{\partial w_{kj}^L} \\ \delta_k^L(t) = y_k(t) - o_k^L(t) \\ \frac{\partial o_k^L(t)}{\partial w_{kj}^L} = \sigma'(net_k^L(t)) o_j^{L-1}(t) + \sum_{d=1}^{D} a_{kd}^L \frac{\partial o_k^L(t-d)}{\partial w_{kj}^L} \end{cases} . \quad (3)$$

For SISO systems, we have $N^L = K = 1$. The term $\frac{\partial o_k^L(t)}{\partial w_{kj}^L}$ is calculated recursively by initially assigning some random values to $\frac{\partial o_k^L(t-d)}{\partial w_{kj}^L}$ for $d = 1, 2, \cdots, D$ [9, 10].

$$\begin{cases} \Delta a_{kd}^L = \eta\, \delta_k^L(t) \frac{\partial o_k^L(t)}{\partial a_{kd}^L} \\ \delta_k^L(t) = y_k(t) - o_k^L(t) \\ \frac{\partial o_k^L(t)}{\partial a_{kd}^L} = o_k^L(t-d) + \sum_{d=1}^{D} a_{kd}^L \frac{\partial o_k^L(t-d)}{\partial a_{kd}^L} \end{cases} \quad (4)$$

2.3.2 Hidden Layer Adaptation Laws
The following update laws are derived for the weights and filter parameters in the hidden layers [9, 10].

$$\begin{cases} \Delta w_{ji}^l = \eta\, \delta_j^l(t) \frac{\partial o_j^l(t)}{\partial w_{ji}^l} \\ \delta_j^l(t) = \sum_{n=1}^{N^{l+1}} \delta_n^{l+1}(t) \frac{\partial o_n^{l+1}(t)}{\partial o_j^l(t)} \\ \frac{\partial o_n^{l+1}(t)}{\partial o_j^l(t)} = \sigma'(net_n^{l+1}(t)) w_{nj}^{l+1} + \sum_{d=1}^{D} a_{nd}^{l+1} \frac{\partial o_n^{l+1}(t-d)}{\partial o_j^l(t)} \\ \frac{\partial o_j^l(t)}{\partial w_{ji}^l} = \sigma'(net_j^l(t)) o_i^{l-1}(t) + \sum_{d=1}^{D} a_{jd}^l \frac{\partial o_j^l(t-d)}{\partial w_{ji}^l} \end{cases} \quad (5)$$

$$\begin{cases} \Delta a_{jd}^l = \eta\, \delta_j^l(t) \frac{\partial o_j^l(t)}{\partial a_{jd}^l} \\ \delta_j^l(t) = \sum_{n=1}^{N^{l+1}} \delta_n^{l+1}(t) \frac{\partial o_n^{l+1}(t)}{\partial o_j^l(t)} \\ \frac{\partial o_n^{l+1}(t)}{\partial o_j^l(t)} = \sigma'(net_n^{l+1}(t)) w_{nj}^{l+1} + \sum_{d=1}^{D} a_{nd}^{l+1} \frac{\partial o_n^{l+1}(t-d)}{\partial o_j^l(t)} \\ \frac{\partial o_j^l(t)}{\partial a_{jd}^l} = o_j^l(t-d) + \sum_{d=1}^{D} a_{jd}^l \frac{\partial o_j^l(t-d)}{\partial a_{jd}^l} \end{cases} \quad (6)$$

2.4 Identification of a More General Class of Nonlinear Systems

As mentioned earlier, the dynamic neural network described in the previous subsection has the capability of identifying the nonlinear system in the form of (1). However, many nonlinear systems may not be represented by system (1). In [9, 10], the generalization of the neural network to three more classes of nonlinear systems has been developed. Here, we describe the extension of the results to the nonlinear system in the form

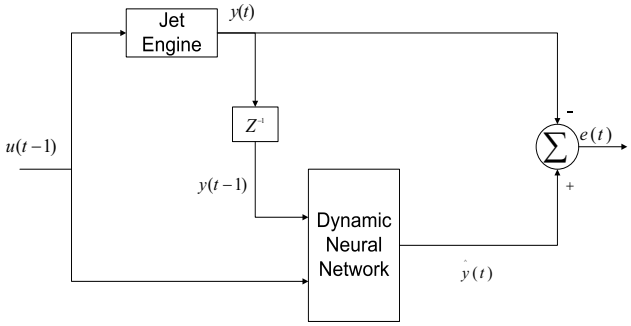

FIGURE 4. A SERIES-PARALLEL DYNAMIC NEURAL NETWORK ARCHITECTURE FOR IDENTIFYING A CLASS OF NONLINEAR SYSTEMS.

$$y(t) = f[y(t-1), \cdots, y(t-N_s), u(t-1), \cdots, u(t-M_s)] \quad (7)$$

where $M_s \leq N_s$. The dynamic behavior of gas turbine engines in our work has been assumed to belong to this class of nonlinear systems.

A series-parallel architecture is used in [9, 10] to develop a neuro-dynamic structure for identifying the class of nonlinear systems in the form of (7). Figure 4 shows the structure of the dynamic neural network. A multilayer feedforward structure with two inputs is used to approximate the nonlinearity $f(\cdot)$ in (7). We have [9, 10]

$$o_i^1(t) = \sum_{d=1}^{D} a_{id}^1 o_i^1(t-d) + \sigma(w_{i1}^1 x_1(t-1) + w_{i2}^1 x_2(t-1)) \quad (8)$$

where $x_1(t-1)$ and $x_2(t-1)$ are the inputs to the network. By substituting o_i^1 in o_j^2, we obtain [9, 10]

$$o_j^2(t) = \sum_{d=1}^{D} a_{jd}^2 o_j^2(t-d) + \sigma[\sum_{i=1}^{N^1} w_{ji}^2 (\sum_{d=1}^{D} a_{id}^1 o_i^1(t-d) + \sigma(w_{i1}^1 x_1(t-1) + w_{i2}^1 x_2(t-1))] \quad (9)$$

The second term in (9) contains o_i^1 to $o_i^1(t-D)$ terms, and $o_i^1(t-d)$ contains $x_1(t-d)$ and $x_2(t-d)$. Therefore, equation (9) can

be rewritten as [9, 10]

$$o_j^2(t) = \sum_{d=1}^{D} a_{jd}^2 o_j^2(t-d) + \psi[x_1(t-1), \cdots, x_1(t-1-D), \cdots, x_2(t-1), \cdots, x_2(t-1-D), \cdots] \tag{10}$$

where ψ is a lower and upper bounded nonlinear function. Similarly, we can show that the output of the last layer is [9, 10]

$$o_j^L(t) = \sum_{d=1}^{D} a_{jd}^L o_j^L(t-d) + \Lambda_f[x_1(t-1), \cdots, x_1(t-p), \cdots, x_2(t-1), \cdots, x_2(t-q)] \tag{11}$$

where Λ_f is to approximate $f(\cdot)$ and p and q are arbitrary large numbers. By substituting $x_1(t-1) = y(t-1)$, $x_2(t-1) = u(t-1)$, $p = N_s$ and $q = M_s$ in (11), we obtain [9, 10]

$$o_j^L(t) = \sum_{d=1}^{D} a_{jd}^L o_j^L(t-d) + \Lambda_f[y(t-1), \cdots, y(t-N_s), \cdots, u(t-1), \cdots, u(t-M_s)] \tag{12}$$

Comparing the output of the nonlinear system (7) with the output of the dynamic network given by equation (12), we realize that in order to identify the nonlinear system (7), the filters have to be removed from the output layer, i.e., $a_{jd}^L = 0$ [9, 10]. We also must have $L \geq 2$. The update laws for the network are similar to those presented in the previous section. A discussion on the stability of the update laws has been presented in [9, 10].

3 Jet Engine Mathematical Model

A nonlinear mathematical model for a dual spool jet engine is developed. For transient response modeling of the jet engine, rotor dynamics and volume dynamics are considered. In order to take into account the volume dynamics, the engine components are assumed to be volume-less and a volume among components is considered to model an imbalance mass flow rate [13]. This modeling consideration allows the elimination of large algebraic loops and provides a reasonable ground for development of a generic and a modular model of the jet engine dynamics. The modules and the information flow amongst the various components for a dual spool engine is shown in Figure 5. In the following, detailed mathematical expressions corresponding to the engine dynamics as well as each specific component are presented.

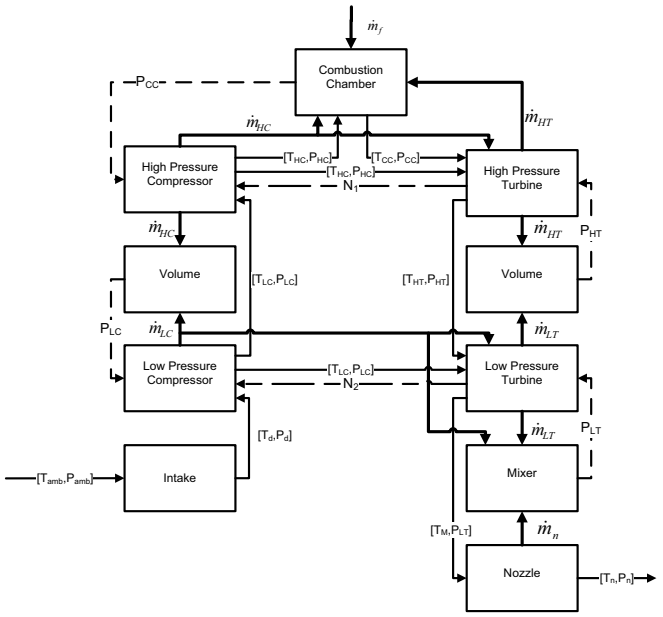

FIGURE 5. INFORMATION FLOW DIAGRAM IN A MODULAR MODELING OF THE JET ENGINE DYNAMICS.

3.1 Rotor Dynamics

Energy balance between the shaft and the compressor results in the following differential equation:

$$\frac{dE}{dt} = \eta_{mech} W_T - W_C \tag{13}$$

where $E = \frac{J(\frac{N.2\pi}{60})^2}{2}$. Refer to the nomenclature section for specific definitions of the various terms and variables.

3.2 Volume Dynamics

As mentioned above, the volume dynamics is considered to take into account the unbalance mass flow rates among various components. Assuming that the gas has zero speed and has homogenous properties over volumes, this dynamics can be described by the following equation:

$$\dot{P} = \frac{RT}{V}(\Sigma \dot{m}_{in} - \Sigma \dot{m}_{out}) \tag{14}$$

3.3 Components

3.3.1 Compressor

The compressor behavior, as a quasi-steady component, is determined by using the compressor performance map (this map is obtained from the commercial software package GSP [14]). Given the pressure ratio (π_C) and the corrected rotational speed

$(N/\sqrt{\theta})$, one can obtain the corrected mass flow rate $(\dot{m}_C\sqrt{\theta}/\delta)$ and efficiency (η_C) from the performance map by using a proper interpolation technique, where $\theta = T_i/T_0$ and $\delta = P_i/P_0$, i.e. $\dot{m}_C\sqrt{\theta}/\delta = f_{\dot{m}_C}(N/\sqrt{\theta}, \pi_C)$ and $\eta_C = f_{\eta_C}(N/\sqrt{\theta}, \pi_C)$. Once these parameters are obtained, the compressor temperature rise and the mechanical power are obtained as follows:

$$T_o = T_i\left[1 + \frac{1}{\eta_C}(\pi_C^{\frac{\gamma-1}{\gamma}} - 1)\right] \tag{15}$$

$$W_C = \dot{m}_C c_p (T_o - T_i) \tag{16}$$

3.3.2 Turbine

Similar to the compressor, the turbine behavior is also determined by using the turbine performance map (from the software package GSP [14]). Given the pressure ratio (π_T) and the corrected rotational speed $(N/\sqrt{\theta})$, the corrected mass flow rate $(\dot{m}_T\sqrt{\theta}/\delta)$ and the efficiency (η_T) are obtained from the performance map, i.e. $\dot{m}_T\sqrt{\theta}/\delta = f_{\dot{m}_T}(N/\sqrt{\theta}, \pi_T)$ and $\eta_T = f_{\eta_T}(N/\sqrt{\theta}, \pi_T)$. The temperature drop and the turbine mechanical power are obtained as follows:

$$T_o = T_i\left[1 - \eta_T(1 - \pi_T^{\frac{\gamma-1}{\gamma}})\right] \tag{17}$$

$$W_T = \dot{m}_T c_p (T_i - T_o) \tag{18}$$

3.3.3 Combustion Chamber

The dynamics inside the combustion chamber is governed by equations (19) and (20). In fact, the combustion chamber represents both the energy accumulation and the volume dynamics between the high pressure compressor and the high pressure turbine at the same time. In other words, we have

$$\dot{P}_{CC} = \frac{P_{CC}}{T_{CC}}\dot{T}_{CC} + \frac{\gamma R T_{CC}}{V_{CC}}(\dot{m}_C + \dot{m}_f - \dot{m}_T) \tag{19}$$

$$\begin{aligned}\dot{T}_{CC} = &\frac{1}{c_v m_{CC}}[(c_p T_C \dot{m}_C + \eta_{CC} H_u \dot{m}_f - c_p T_{CC}\dot{m}_T) - \\ &c_v T_{CC}(\dot{m}_C + \dot{m}_f - \dot{m}_T)]\end{aligned} \tag{20}$$

3.4 Set of Nonlinear Equations

In this section, a set of nonlinear equations corresponding to a dual spool jet engine is provided. In the engine intakes, by assuming adiabatic process, the pressure and the temperature are computed as follows:

$$\frac{P_d}{P_{amb}} = \left[1 + \eta_d \frac{\gamma-1}{2}M^2\right]^{\frac{\gamma}{\gamma-1}} \tag{21}$$

$$\frac{T_d}{T_{amb}} = 1 + \frac{\gamma-1}{2}M^2 \tag{22}$$

For a low pressure compressor, the pressure ratio π_{LC} is calculated from the volume dynamics between the high pressure compressure and the low pressure compressor as described by equation (14). The rotational speed (N_2) is obtained from the solution to equation (13) for the spool that is connecting the low pressure compressor to the low pressure turbine. According to the pressure ratio and the rotational speed, the corrected mass flow and the efficiency are obtained from the performance map, therefore the temperature rise can be obtained from equation (15). Similar to the low pressure compressor, for high pressure compressor, pressure is obtained from the volume dynamics that is described by equation (19). The rotational speed (N_1) is obtained from equation (13) for a spool that is connecting the high pressure compressor to the high pressure turbine.

Finally, the pressure ratio of high pressure turbine is obtained from the volume dynamics between the high and the low pressure turbines, and the pressure ratio for the low pressure turbine is calculated by using the volume dynamics after the low pressure turbine. The mass flow rate of the nozzle is computed as follows. If condition (23) holds, the mass flow rate is obtained from equation (24), otherwise, it is determined from equation (25). In other words, we have

$$\frac{P_{amb}}{P_{n_i}} < \left[1 + \frac{1-\gamma}{\eta_n(1+\gamma)}\right]^{\frac{\gamma}{\gamma-1}} \tag{23}$$

$$\frac{\dot{m}_n\sqrt{T_{n_i}}}{P_{n_i}} = \frac{u}{\sqrt{T_{n_i}}}\frac{A_n}{R}\frac{P_{amb}}{P_{n_i}}\frac{T_{n_i}}{T_{n_o}} \tag{24}$$

where $\frac{u}{\sqrt{T_{n_i}}} = \sqrt{2c_p\eta_n(1-(\frac{P_{amb}}{P_{n_i}})^{\frac{\gamma-1}{\gamma}})}$, $\frac{T_{no}}{T_{n_i}} = 1 - \eta_n(1 - (\frac{P_{amb}}{P_{n_i}})^{\frac{\gamma-1}{\gamma}})$, and

$$\frac{\dot{m}_n\sqrt{T_{n_i}}}{P_{n_i}} = \frac{u}{\sqrt{T_{n_i}}}\frac{A_n}{R}\frac{P_{crit}}{P_{n_i}}\frac{T_{n_i}}{T_{crit}} \tag{25}$$

and where $\frac{P_{crit}}{P_{n_i}} = (1-\frac{1}{\eta_n}(\frac{\gamma-1}{\gamma+1}))^{\frac{\gamma}{\gamma-1}}$, $\frac{u}{\sqrt{T_{n_i}}} = \frac{2\gamma R}{\gamma+1}$, and $\frac{T_{crit}}{T_{n_i}} = \frac{2}{\gamma+1}$. Here, it is assumed that $P_{n_i} = P_{LT}$ and $T_{n_i} = T_M$ which is obtained from of energy balance in the mixer as follows:

$$T_M = \frac{\dot{m}_{LT}T_{LT} + \beta\dot{m}_{LC}T_{LC}}{\dot{m}_{LT} + \beta\dot{m}_{LC}}$$

Also the input or the control signal is $u = PLA$ which is related to fuel flow rate by a gain, i.e. $\dot{m}_f = PLA \times \dot{m}_f^{max}$, where $\dot{m}_f^{max}$ is the maximum fuel flow rate. Moreover, all the performance maps of the compressors and the turbines are adopted from the commercial software package GSP [14].

4 FAULT DETECTION IN GAS TURBINE ENGINES

In this section, a fault detection methodology for a dual-spool jet engine by using the dynamic neural network structure described in Section 2 is developed. Before proceeding to fault detection in the jet engine, we briefly describe the concept of fault detection in dynamical systems.

4.1 Problem of Fault Detection

The purpose of a fault detection mechanism in dynamical systems is to detect faults after they occur and before they evolve into failures. Generally, for detecting a fault in a system, some sort of redundancy is required. Hardware redundancy is a conventional approach for fault detection. In this approach, multiple sensors or actuators are utilized to measure and control a variable of interest in a dynamical system. Typically, a voting mechanism is utilized to determine if a fault has occurred. Due to the use of redundant hardware, hardware redundancy approaches can become very costly.

Fault detection approaches based on analytical redundancy have attracted a great deal of attention. In analytical redundancy methods, the inherent redundancy existing in the static and dynamic relationships among the system inputs and measured outputs is used for fault detection and isolation. In other words, sensor measurements are compared with the values of the respective variables which are obtained analytically based on a mathematical model of the system or through the process of historical data. The resulting differences are called **residuals**. The residuals are processed to determine which residuals can be considered normal and which ones indicate presence of a fault. When no fault is present in the system, the residual should be normally zero or very close to zero, and when a fault occurs, the residual should be distinguishably different from zero and above a specific threshold. The algorithm or processor used to generate residuals is called a **residual generator**.

The fault detection approaches based on analytical redundancy can be categorized into model-based and computationally intelligence-based schemes. In the model-based approaches, a mathematical representation of the system is assumed to be available. In contrast, in intelligence-based approaches, fault detection is achieved via the process of historical data. Neural networks have been widely used as a powerful intelligence-based technique for fault detection using the history of a system's generated data.

TABLE 1. FAULTS CONSIDERED IN THE ENGINE.

Component Fault	Description
f_eLC	Change in the low pressure compressor efficiency
f_eHC	Change in the high pressure compressor efficiency
f_mLT	Change in the low pressure turbine flow capacity

4.2 Engine Component Faults

In this paper, we study three component faults in the engine. Component faults can be modeled as changes in the component efficiency and flow capacity. Table 1 shows the component faults that are studied in this paper and their description.

4.3 Residual Generation

We first train the the neural network with a set of healthy data. Since the network has learned the behavior of the engine, it can be used for residual generation by comparing the engine output with the neural network output. The fault detection algorithm developed in this paper consists of two phases that are explained below.

1- Training Phase

As stated in Section 2, the jet engine studied in this work is assumed to belong to the class of nonlinear systems represented by the input-output relation (7). Therefore, the structure of Figure 4 is used for training the network. In this paper, three dynamic neural networks are developed and trained for modeling and representing the dynamics of three engine outputs N_1, N_2 and T_{CC}. The inputs to each network for training processes are the fuel mass flow rate to the combustion chamber and the one step delay of the actual output of the jet engine.

1- Recall and Residual Generation Phase

In this phase, instead of the plant output, the one step delayed output of the network is fed into the network. Figure 6 shows the architecture of the network at the recall and the fault detection phase.

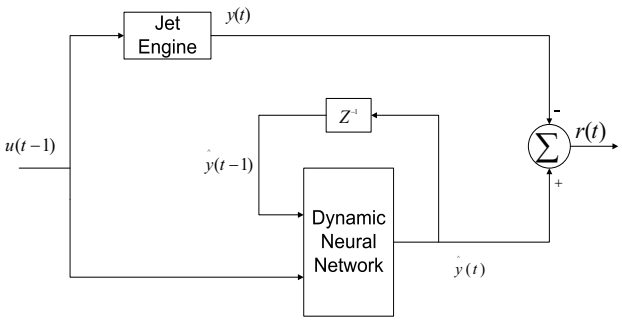

FIGURE 6. THE STRUCTURE OF THE DYNAMIC NEURAL NETWORK FOR THE GENERALIZATION AND FAULT DETECTION.

4.3.1 Threshold Selection

For fault detection purposes, a threshold testing process is fulfilled. In this process, the network is tested with arbitrary random inputs and the residual signals generated at each test (assuming healthy operation of the engine) are processed to find an appropriate threshold for accomplishing the fault detection task during the faulty operation of the engine.

5 SIMULATION RESULTS

For simplicity of discussions, we denote the network structures developed to represent N_1, N_2 and T_{CC} by Net_{N_1}, Net_{N_2} and $Net_{T_{CC}}$, respectively. We assume the ground ambient conditions.

5.1 Training Data

In this work, we assume that the minimum fuel mass flow rate that must be supplied to the combustion chamber for the engine operation and in order to avoid the engine flame out is 45% of the maximum fuel mass flow rate. The engine is assumed fault-free at the training phase. As mentioned in the previous section, three dynamic neural networks are developed and trained to represent three engine outputs N_1, N_2 and TCC. We trained the networks with different input profiles, and we observed that if a step input with the amplitude equal to the 75% of the maximum fuel mass flow rate is used for training each network, a smaller steady state error between the network output and the engine output can be achieved. Each network is trained with a set of 200 normalized data points. The data points are normalized to a zero mean and standard deviation of one.

5.2 Network Parameters

The initial filter parameters are taken to be small (about 0.01). The initial weights for all the networks are considered to be 0.25. The parameters of the networks have been selected to generate an optimized output with minimal steady state error between the network output and the engine output. The network parameters are shown in Table 2. Here, η_w and η_a are the different learning rates used for updating the network weights and filter parameters, respectively. The steady state error of each network for different input values is shown in Table 3. In Table 3, w_i represents the input fuel mass flow rate and W_{max} denotes the maximum fuel mass flow rate.

TABLE 2. NETWORKS' PARAMETERS.

	Net_{N_1}	Net_{N_2}	$Net_{T_{CC}}$
D	3	2	3
L	3	3	3
N^1	3	3	20
N^2	6	4	6
η_w	0.14	0.05	0.11
η_a	0.15	0.12	0.21

TABLE 3. STEADY-STATE ERROR OF THE NETWORK OUTPUT AND THE ENGINE OUTPUT.

	$\lvert e_{ss}\rvert$ when $w_i = 0.50W_{max}$	$\lvert e_{ss}\rvert$ when $w_i = 0.60W_{max}$	$\lvert e_{ss}\rvert$ when $w_i = 0.75W_{max}$	$\lvert e_{ss}\rvert$ when $w_i = 0.80W_{max}$	$\lvert e_{ss}\rvert$ when $w_i = 0.90W_{max}$	$\lvert e_{ss}\rvert$ when $w_i = W_{max}$
Net_{N_1}	6.5 RPM	10.2 RPM	0.46 RPM	5.6 RPM	22.9 RPM	43.8 RPM
Net_{N_2}	10.8 RPM	15.2 RPM	0.26 RPM	11.2 RPM	33.8 RPM	60.9 RPM
$Net_{T_{CC}}$	0.57 K	1.1 K	0.13 K	1.2 K	3.7 K	6.9 K

5.3 Selection of Thresholds for Fault Detection

For the recall and the fault detection tasks, the inputs to the networks are the system fuel mass flow rate and the one step delayed of the network output. For each network, we tested the network with different input fuel mass flow rates and calculated a threshold. The threshold for fault detection for each network is obtained by taking the maximum of the steady state error of each network and multiplied it by a safety factor of 1.2. The thresholds are calculated to be 52 RPM for the residual generated by the network developed to model N_1, 72 RPM for the residual generated by the network developed to model N_2, and 8.5K for the residual generated by the network developed to represent T_{CC}.

5.3.1 Fault Cases Studied

Many fault cases have been studied. The fault cases presented here all correspond to the maximum fuel mass flow rate and 65% maximum fuel mass flow rate.

Fault Case 1- High-pressure compressor efficiency drops 3 % at t=6 *sec*. **when the input fuel mass flow rate is at 65%**

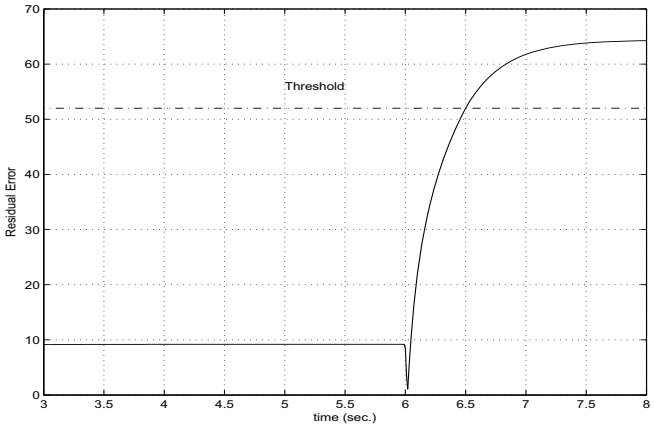

FIGURE 7. RESIDUAL SIGNAL GENERATED BY THE NETWORK REPRESENTING N_1 FOR THE FAULT CASE 1.

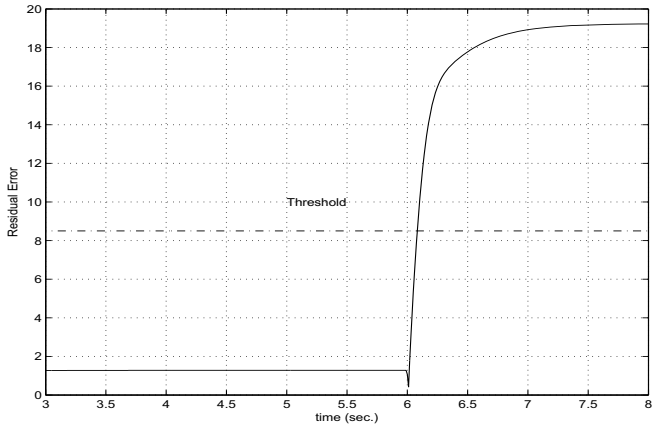

FIGURE 9. RESIDUAL SIGNAL GENERATED BY THE NETWORK REPRESENTING T_{CC} FOR THE FAULT CASE 1.

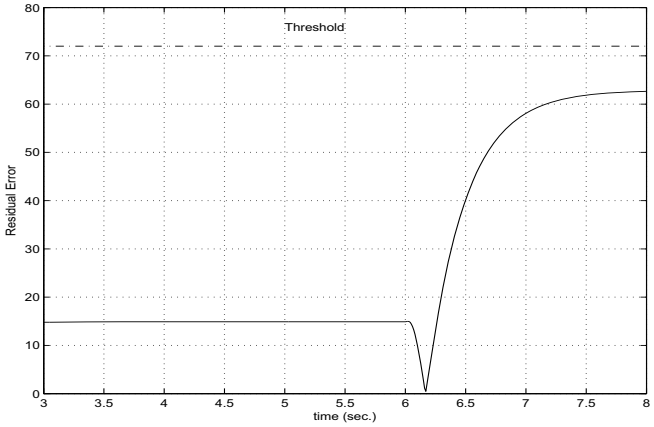

FIGURE 8. RESIDUAL SIGNAL GENERATED BY THE NETWORK REPRESENTING N_2 FOR THE FAULT CASE 1.

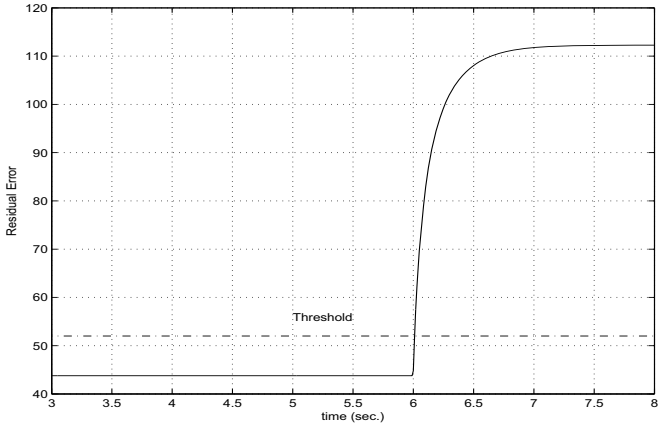

FIGURE 10. RESIDUAL SIGNAL GENERATED BY THE NETWORK REPRESENTING N_1 FOR THE FAULT CASE 2.

of its maximum - Figures 7, 8 and 9 show the residual signals generated by Net_{N_1}, Net_{N_2} and $Net_{T_{CC}}$, respectively. As seen the residuals generated by Net_{N_1} and $Net_{T_{CC}}$ are above the considered thresholds, however, the residual generated by Net_{N_2} is not above its threshold. This implies that Net_{N_2} is generating a false positive, however, the fault is detected if a voting mechanism is used. The detection time for Net_{N_1} is 0.51 *sec*. and for $Net_{T_{CC}}$ is 0.1 *sec*.

Fault Case 2- High-pressure compressor efficiency drops 3 % at t=6 *sec*. **when the input fuel mass flow rate is at its maximum -** Figures 10 and 11 show the residuals generated by the networks Net_{N_1} and $Net_{T_{CC}}$, respectively. The residual generated by Net_{N_2} is not above its threshold and is not shown. Similar to case 1, the fault can be detected. The detection time for Net_{N_1} is 0.03 *sec*. and for $Net_{T_{CC}}$ is 0.02 *sec*.

Fault Case 3- Low-pressure compressor efficiency drops 5% at t=6 sec. when the input fuel mass flow rate is at 65% of its maximum - Figures 12 and 13 show the residuals generated by the networks Net_{N_2} and $Net_{T_{CC}}$, respectively. The residual generated by Net_{N_1} is not above its threshold and is not shown. Similar to the previous two cases, the fault can be detected. The detection time for Net_{N_2} is 0.1 *sec*. and for $Net_{T_{CC}}$ is 0.04 *sec*.

Fault Case 4- Low-pressure compressor efficiency drops 5% at t=6 sec. when the input fuel mass flow rate is at its maximum - Figures 14 and 15 show the residuals generated by the networks Net_{N_2} and $Net_{T_{CC}}$, respectively. The residual generated by Net_{N_1} is not above its threshold and is not shown. Similar to the previous three cases, the fault can be detected using a voting mechanism. The detection time for Net_{N_2} is 0.04 *sec*. and for $Net_{T_{CC}}$ is 0.02 *sec*.

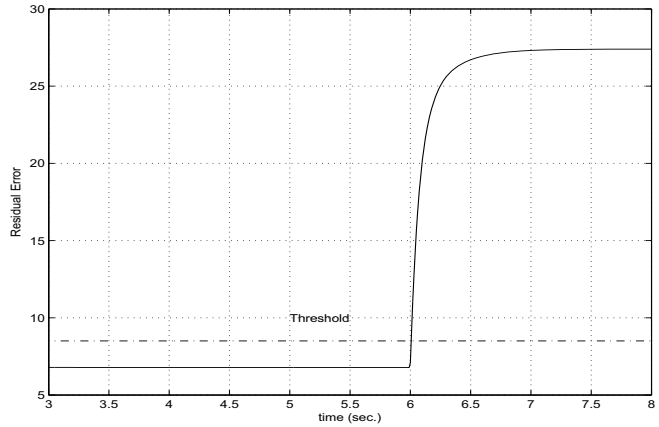

FIGURE 11. RESIDUAL SIGNAL GENERATED BY THE NETWORK REPRESENTING T_{CC} FOR THE FAULT CASE 2.

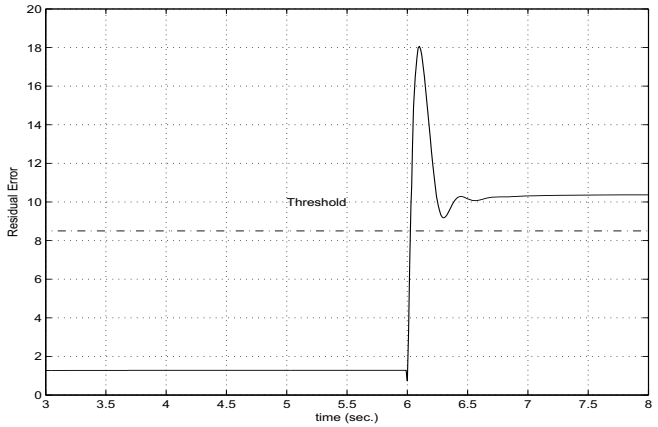

FIGURE 13. RESIDUAL SIGNAL GENERATED BY THE NETWORK REPRESENTING T_{CC} FOR THE FAULT CASE 3.

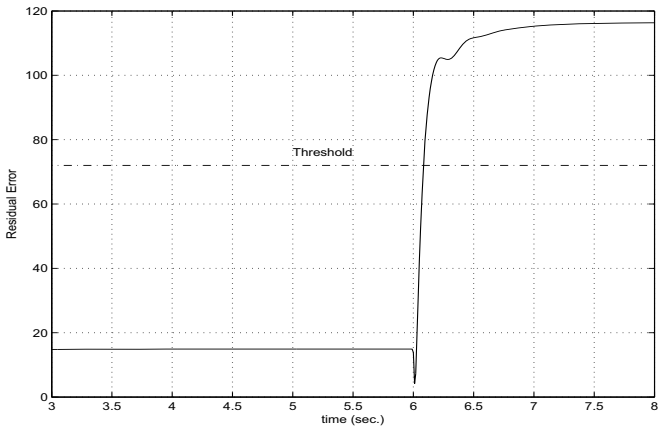

FIGURE 12. RESIDUAL SIGNAL GENERATED BY THE NETWORK REPRESENTING N_2 FOR THE FAULT CASE 3.

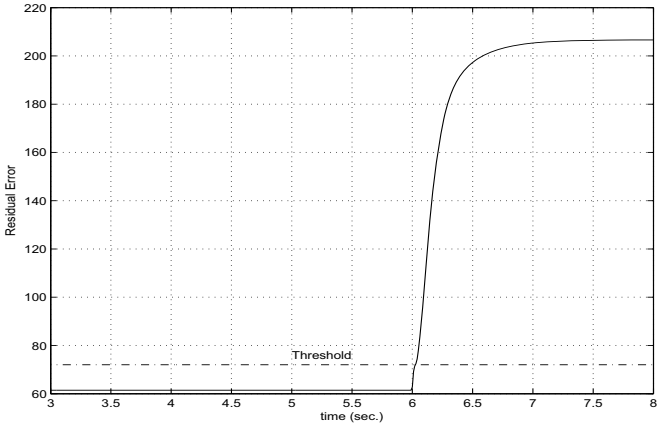

FIGURE 14. RESIDUAL SIGNAL GENERATED BY THE NETWORK REPRESENTING N_2 FOR THE FAULT CASE 4.

Fault Case 5- Low-pressure turbine flow capacity drops 6% at t=6 sec. when the input fuel mass flow rate is at 65% of its maximum - Figures 16 and 17 show the residuals generated by the networks Net_{N_1} and $Net_{T_{CC}}$, respectively. The residual generated by Net_{N_2} is not above its threshold and is not shown. The fault can be detected using a voting mechanism. The detection time for Net_{N_1} is 0.47 *sec*. and for $Net_{T_{CC}}$ is 0.22 *sec*.

Fault Case 6- Low-pressure turbine flow capacity drops 6% at t=6 sec. when the input fuel mass flow rate is at its maximum - All the residual signals generated by the networks are above their thresholds for this case. Figures 18 shows the residual generated by the network Net_{N_1}. The detection time for Net_{N_1} is 0.04 *sec*. For brevity, the residuals generated by Net_{N_2} and $Net_{T_{CC}}$ have not been shown.

5.4 Network Fault Detection Performance

We have injected the faults at different fuel mass flow rates and tested the fault detection capability of the networks. Table 4 shows the minimum values of the faults that can be detected by each network.

5.4.1 Fault Detection in the Presence of Measurement Noise

We have also tested the performance of the networks for the case that measurement noise is present in the engine. We have assumed that the data used for training the networks was noise-free. The measurement noise affects the residuals generated by the networks in such a way that residual signals close to a threshold may pass the threshold. Under this situation, a false alarm

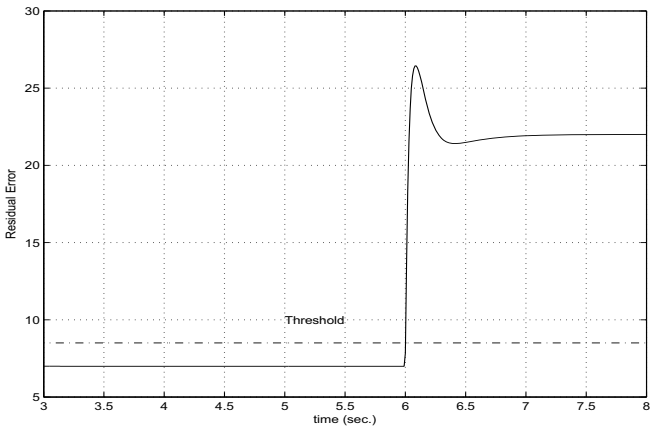

FIGURE 15. RESIDUAL SIGNAL GENERATED BY THE NETWORK REPRESENTING T_{CC} FOR THE FAULT CASE 4.

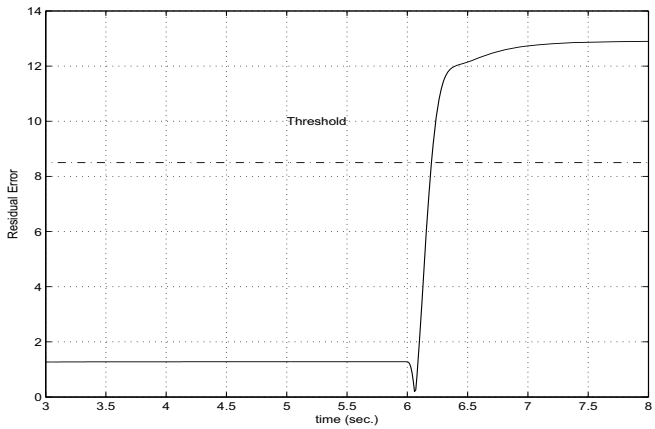

FIGURE 17. RESIDUAL SIGNAL GENERATED BY THE NETWORK REPRESENTING T_{CC} FOR THE FAULT CASE 5.

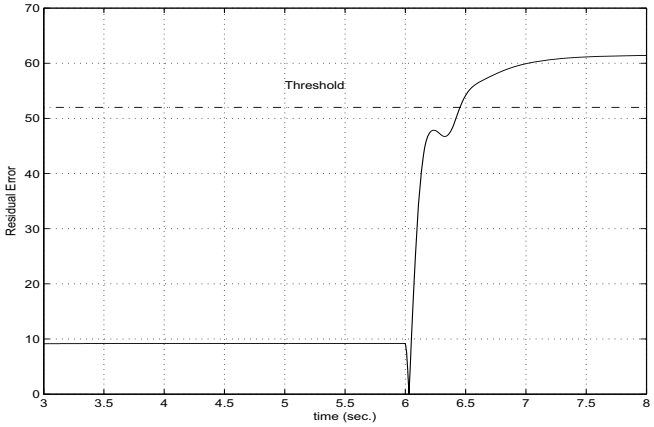

FIGURE 16. RESIDUAL SIGNAL GENERATED BY THE NETWORK REPRESENTING N_1 FOR THE FAULT CASE 5.

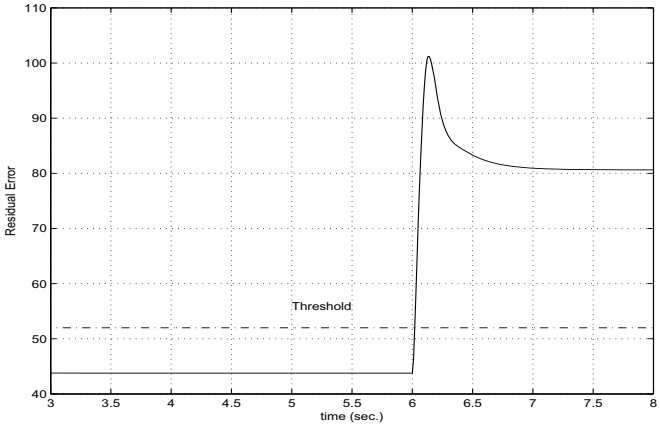

FIGURE 18. RESIDUAL SIGNAL GENERATED BY THE NETWORK REPRESENTING N_1 FOR THE FAULT CASE 6.

or a false positive may be generated by the fault detection system. As mentioned earlier in this section, we choose thresholds with a safety factor. This may reduce the effect of noise on the fault detection results. However, if the magnitude of noise is large, the residual may become unreliable. This may increase the minimum values of the faults that can be detected using each network. Figure 19 shows the response of $Net_{T_{CC}}$ for the case that the low-pressure turbine flow capacity drops 6% at t=6 sec. when the input fuel mass flow rate is at 65% of its maximum, and a measurement noise with the magnitude equal to the 6% of the maximum measured T_{CC} is present. In the presence of the measurement noise considered, the minimum low-pressure turbine flow capacity drop that can be detected by $Net_{T_{CC}}$ is 4%. Table 5 shows the minimum value of the faults that can be detected by the networks in the presence of 6% measurement noise.

6 CONCLUSION

In this paper, we have investigated the fault detection of gas turbine engines and presented a novel approach based on dynamic neural networks. Dynamic neural networks, in contrast to the conventional neural networks, are composed of dynamic neurons. In dynamic neurons, there is a digital filter after the activation function that generates a dynamic mapping between the input and output of the neuron. The dynamic neurons, when used in a multilayer feedforward neural network structure, create a strong tool for identification of nonlinear systems. The identification capabilities of dynamic neural networks is used in this paper for fault detection in gas turbine engines. The structure of the dynamic neural networks has been investigated and their update laws have been reviewed. Three dynamic neural networks have been developed for representing the engine output signals

TABLE 4. MINIMUM VALUE OF THE FAULTS THAT CAN BE DETECTED BY THE NETWORKS.

Component Fault	Minimum fault detected by using Net_{N_1}	Minimum fault detected by using Net_{N_2}	Minimum fault detected by using $Net_{T_{CC}}$
f_eLC	7%	4%	2%
f_eHC	3%	9%	2%
f_mLT	6%	8%	2%

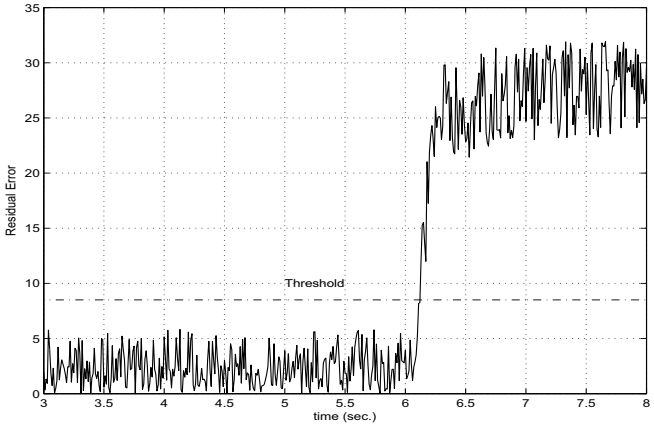

FIGURE 19. RESIDUAL SIGNAL GENERATED BY THE NETWORK REPRESENTING T_{CC} FOR THE CASE THAT THE LOW-PRESSURE TURBINE FLOW CAPACITY DROPS 6% AT t=6 sec. WHEN THE INPUT FUEL MASS FLOW RATE IS AT 65% OF ITS MAXIMUM AND 6% MEASUREMENT NOISE IS PRESENT.

TABLE 5. MINIMUM VALUE OF THE FAULTS THAT CAN BE DETECTED BY THE NETWORKS IN THE PRESENCE OF 6% MEASUREMENT NOISE.

Component Fault	Minimum fault detected by using Net_{N_1}	Minimum fault detected by using Net_{N_2}	Minimum fault detected by using $Net_{T_{CC}}$
f_eLC	10%	7%	4%
f_eHC	5%	12%	4%
f_mLT	9%	12%	4%

N_1, N_2 and T_{CC}. The performance of the neural networks has been investigated by some illustrative fault cases.

The development of dynamic neural networks for modeling other engine variables is an ongoing task. The applicability of the presented neural networks for fault isolation and in particular, the integration of Radial Basis Functions (RBF) in our proposed network structure for achieving a very competitive fault isolation requirement is the subject of our future research.

REFERENCES

[1] Litt, J. S., Simon, D. L., Garg, S., Guo, T.-H., Mercer, C., Millar, R., Behbahani, A., Bajwa, A., and Jensen, D. T., 2005. "A survey of intelligent control and health management technologies for aircraft propulsion systems," *NASA Technical report*, NASA/TM-2005-213622.

[2] Tumer, I. Y., and Bajwa, A., 1999. "A survey of aircraft engine health monitoring systems," *35th AIAA/ASME/SAE/ASEE Joint Propulsion Conf. and Exhibit*, Los Angeles, CA, USA, AIAA-99-2528.

[3] Jaw, L. C., 2005. "Recent advancements in aircraft engine health management (EHM) technologies and recommendations for the next step," *Proc. of Turbo Expo 2005*, Reno-Tahoe, NV, USA.

[4] Patton, R. J., and Chen, J., 1991. "Detection of faulty sensors in aero jet engine systems using robust model-based methods," *IEE Colloquium on Condition Monitoring for Fault Diagnosis*, pp. 2/1-2/22.

[5] Kobayashi, T., and Simon, D. L., 2003. "Application of a bank of Kalman filters for aircraft engine fault diagnostics," *Proc. of ASME Turbo Expo 2003*, Atlanta, GA, USA.

[6] Dai, X., Breikin, T., Gao, Z., and Hong, W., 2008. "Dynamic modelling and robust fault detection of a gas turbine engine," *Proc. of the American Control Conf.*, Seattle, WA, USA, pp. 2160-2165.

[7] Hajiyev, C., and Kaliskan, F., 2000. "Sensor/actuator fault diagnosis based on statistical analysis of innovation sequence and robust Kalman filtering," *Aerospace Science & Technology*, vol. 4, pp. 415-422.

[8] Mohammadi, R., Hashtrudi-Zad, S., and Khorasani, K., 2009."Hybrid fault diagnosis: Application to a gas turbine engine," *Proc. of Turbo Expo 2009*, Orlando, FL, USA.

[9] Yazdizadeh, A., and Khorasani, K., 2002. "Adaptive time delay neural network structure for nonlinear system identification," *NeuroComputing*, Vol. 47, pp. 207-240.

[10] Yazdizadeh, A., and Khorasani, K., 1997. "Identification of a class of nonlinear systems using dynamic neural networks," *IEEE Int. Joint Conf. on Neural Networks*.

[11] Cybenko, G. 1989. "Approximation by superpositions of sigmoidal function," *Mathematics of control, signals and systems*, Vol. 2, pp. 303-314.

[12] McClelland , J.L., and Rumelhart, D.E., 1988. "Parallel Distributed Processing," *The MIT Press*, Vol 1,2, Cambridge, London, England.

[13] Camporeale, S. M., Fortunato, B., and Mastrovito, M., 2006. "A Modular code for real time dynamic simulation of gas turbines in SIMULINK," *Journal of Engineering for Gas Turbines and Power*, Vol. 128, pp. 506-517.

[14] Visser, W. P. J., and Broomhead, M. J., 2000. "GSP, A generic object-oriented gas turbine simulation environment," *International Gas Turbine and Aeroengine Congress and Exposition*.